

Full Torus Electromagnetic Gyrokinetic Particle Simulations with Kinetic Electrons

Y. Nishimura*, Z. Lin and L. Chen

Department of Physics and Astronomy, University of California, Irvine, 92697-4575, USA.

Received 27 December 2007; Accepted (in revised version) 20 May 2008

Available online 15 July 2008

Abstract. The full torus electromagnetic gyrokinetic particle simulations using the hybrid model with kinetic electrons in the presence of magnetic shear is presented. The fluid-kinetic electron hybrid model employed in this paper improves numerical properties by removing the tearing mode, meanwhile, preserves both linear and nonlinear wave-particle resonances of electrons with Alfvén wave and ion acoustic wave.

PACS: 52.20.Gz, 52.35.Ra, 52.65.Cc

Key words: Gyrokinetic particle simulation, plasma turbulence, electromagnetic gyrokinetic theory.

1 Introduction

Anomalous particle and heat transport in magnetized fusion plasma in the electrostatic limits have been studied extensively by three dimensional gyrokinetic turbulence simulations [1, 2]. The ion heat transport driven by ion temperature gradient mode (ITG) [3] and regulation by the zonal flows is well understood [2, 4]. The electron heat transport can be related to trapped electron modes (TEM) [5–7], effective perpendicular transport induced by stochastic magnetic field lines [8, 9], or possibly by electron temperature gradient mode (ETG) [10–12]. On the other hand, in the presence of magnetic perturbations, there exist new branches of modes, for example, toroidicity induced Alfvén eigenmodes (TAEs) [13, 14], Alfvénic ion temperature gradient (AITG) modes [15, 16], and kinetic ballooning modes (KBM) [17], that can play important roles in plasma instabilities and transport.

To predict the particle and heat transport level reliably for the next generation burning plasma experiments, for example for the International Thermonuclear Experimental

*Corresponding author. *Email addresses:* ynishimu@pppl.gov (Y. Nishimura), zhihongl@uci.edu (Z. Lin), liuchen@uci.edu (L. Chen)

Reactor (ITER), it is important to include the electromagnetic effects self-consistently into the gyrokinetic simulation. However, in electromagnetic gyrokinetic particle-in-cell (PIC) simulations [18, 19], freely streaming electrons above the local Alfvén speed greatly enhance particle noise inherent to the electromagnetic gyrokinetic PIC method [20, 21]. A fluid-kinetic hybrid electron model [22–25] has been proposed to circumvent these difficulties. The hybrid model solves for the adiabatic response in the lowest order as massless electron fluid equations and solves the resonant interaction in the higher order kinetic equations, based on an expansion of the electron response using a small parameter of the square-root of the electron-ion mass ratio

$$\delta_m = (m_e/m_i)^{1/2}$$

(m_e and m_i are the electron and the ion mass respectively), while preserving the linear and the nonlinear wave-particle interactions (note, however, that we did not conduct nonlinear simulation in this paper).

The motivation for the development of the hybrid model is to remove the well known numerical difficulty [20, 21] of resolving the electron response to the tearing parity near mode rational surfaces in the presence of magnetic shear. The hybrid model is free from this difficulty by removing the tearing mode physics in our simulations, while the full kinetic model [20, 21] can suffer from the difficulty since the tearing mode is retained. The hybrid model makes approximations at the electron gyroradius scales and removes the $k_{\parallel} = 0$ component of the inductive parallel electric field (here, k_{\parallel} is the wave vector parallel to the equilibrium magnetic field), that is the collisionless tearing mode. However, the hybrid model treats rigorously all other $k_{\parallel} = 0$ modes, including electrostatic fields, magnetic field perturbations, zonal flows and zonal fields, and all the ideal and resistive MHD modes. The hybrid model is optimal for simulation of drift and Alfvénic turbulence on the ion gyroradius scales. The hybrid model does not treat the tearing physics in exchange for better numerical properties when simulating drift-Alfvénic turbulence.

Based on the mathematical derivation by [23, 25] presented a toroidal version of the fluid-kinetic hybrid electron model for treating electron dynamics in electromagnetic gyrokinetic particle simulations. However, the major focus of the numerical calculations in [25] was the examination of the shear Alfvén wave dynamics in global tokamak plasmas with only the fluid hierarchy of the hybrid model (which constructed a closed set of physics discussion employing the lowest order fluid electrons). On the other hand, global toroidal gyrokinetic particle simulations with kinetic electrons using the electrostatic version of the hybrid model were reported [7, 26]. In this paper, the full torus electromagnetic gyrokinetic particle simulations using the hybrid model with kinetic electrons in the presence of magnetic shear are presented. The fluid-kinetic electron hybrid model employed in this paper improves numerical properties by removing the tearing mode. The hybrid model preserves both linear and nonlinear wave-particle resonances of electrons with Alfvén wave and ion acoustic wave (note that we do not perform nonlinear simulations in this paper).

The paper is organized as follows. The formulation of the hybrid model is presented in Section 2. Section 3 discussed electromagnetic simulations with kinetic electrons. We summarize in Section 4.

2 The asymptotic expansion of the electron drift kinetic equation

In this section, we present the asymptotic expansion of the electron drift kinetic equation in the hybrid model [22]. We point out where the tearing parity modes are eliminated. For the completeness of the work, mathematical notations in [25] are repeated (as a consequence, several equations are unavoidably the same).

Before proceeding, we note that the parallel electric field in the hybrid model is represented by

$$E_{\parallel} \equiv -\nabla_{\parallel} \Phi_{eff} = -\nabla_{\parallel} \Phi - c^{-1} \partial_t A_{\parallel} = -\nabla_{\parallel} \Phi + \nabla_{\parallel} \Phi_{ind} \quad (2.1)$$

which contains both the electrostatic part and the induction part, and we introduce the *induction* potential Φ_{ind} and the *effective* potential Φ_{eff} , with Φ being the electrostatic potential, and A_{\parallel} is the parallel component of the vector potential. Note that we have imposed $c^{-1} \partial_t A_{\parallel} = -\nabla_{\parallel} \Phi_{ind}$ (c is the speed of light). As we see later this is where the tearing mode physics is eliminated.

In describing the equilibrium magnetic field in the toroidal geometry, we take the Clebsch form

$$\mathbf{B}_0 = \nabla \psi_0 \times \nabla \alpha_0,$$

where ψ_0 is the poloidal flux label and $\alpha_0 = q(\psi_0)\theta - \zeta$ is the magnetic field line label with θ and ζ being the poloidal angle and the toroidal angle, respectively. Here, $q(\psi_0)$ is the equilibrium safety factor. The magnetic field in the presence of the perturbation $\delta\psi(\psi_0, \theta, \zeta, t)$ and $\delta\alpha(\psi_0, \theta, \zeta, t)$ is given by (t denotes the time variable)

$$\mathbf{B} = \mathbf{B}_0 + \delta\mathbf{B} = \nabla(\psi_0 + \delta\psi) \times \nabla(\alpha_0 + \delta\alpha).$$

The magnetic perturbation is also given by $\delta\mathbf{B} = \nabla A_{\parallel} \times \mathbf{b}_0$. Here, we denote $\mathbf{b} = \mathbf{B}/B_0$ and $\mathbf{b}_0 = \mathbf{B}_0/B_0$. The vector potential A_{\parallel} , $\delta\psi$, and $\delta\alpha$ are related through the relations

$$\partial A_{\parallel} / \partial \alpha_0 = -\mathbf{b} \cdot \nabla \delta\psi, \quad (2.2)$$

$$\partial A_{\parallel} / \partial \psi_0 = \mathbf{b} \cdot \nabla \delta\alpha. \quad (2.3)$$

Taking (μ, v_{\parallel}) as independent variables which is implemented in the GTC code [2], the drift kinetic equation [27, 28] is given by

$$\frac{df_e}{dt} = \frac{\partial f_e}{\partial t} + (v_{\parallel} \mathbf{b} + \mathbf{v}_E + \mathbf{v}_g + \mathbf{v}_c) \cdot \nabla f_e - \mathbf{b}^* \cdot \nabla (\mu B - e \Phi_{eff}) \frac{1}{m_e} \frac{\partial f_e}{\partial v_{\parallel}} = 0. \quad (2.4)$$

The magnetic moment is defined by $\mu = m_e v_\perp^2 / 2B$, where the parallel and perpendicular particle velocities are given by v_\parallel and v_\perp , respectively. The $E \times B$ drift velocity is given by

$$\mathbf{v}_E = c \mathbf{B}_0 \times \nabla \Phi / B_0^2,$$

the electron gradient-B drift is given by

$$\mathbf{v}_g = (m_e \Omega_{ce} B_0^2)^{-1} (\mu B_0) \mathbf{B}_0 \times \nabla B_0,$$

the electron curvature drift is given by

$$\mathbf{v}_c = (v_\parallel^2 / \Omega_{ce}) \mathbf{b} \times (\mathbf{b} \cdot \nabla) \mathbf{b}$$

(e is the unit charge, $\Omega_{ce} = -eB_0 / m_e c$ is the electron cyclotron frequency), $\mathbf{b}^* = \mathbf{b} + \mathbf{v}_c / v_\parallel$, and $\mathbf{b}_0^* = \mathbf{b}_0 + \mathbf{v}_c / v_\parallel$. We then separate the electron distribution function into the equilibrium part and the fluctuation part as $f_e = f_{0e} + \delta f_e$. The equilibrium part f_{0e} is defined by

$$\left[\frac{\partial}{\partial t} + (v_\parallel \mathbf{b}_0 + \mathbf{v}_g + \mathbf{v}_c) \cdot \nabla - \mathbf{b}_0^* \cdot \nabla (\mu B) \frac{1}{m_e} \frac{\partial}{\partial v_\parallel} \right] f_{0e} = 0. \quad (2.5)$$

Note that f_{0e} is dependent not only on the flux surface label ψ_0 but also on the poloidal angle θ . The δf_e equation is given by

$$\begin{aligned} \frac{d\delta f_e}{dt} &= -v_\parallel \frac{\delta \mathbf{B}}{B} \cdot \nabla f_{0e} - \mathbf{v}_E \cdot \nabla f_{0e} + \frac{\delta \mathbf{B}}{B} \cdot \nabla (\mu B - e\Phi_{eff}) \frac{1}{m_e} \frac{\partial f_{0e}}{\partial v_\parallel} - \mathbf{b}_0^* \cdot \nabla (-e\Phi_{eff}) \frac{1}{m_e} \frac{\partial f_{0e}}{\partial v_\parallel} \\ &= \frac{c}{B^2} \mathbf{B} \cdot \nabla f_{0e} \times \left(\nabla \Phi - v_\parallel \nabla \frac{A_\parallel}{c} \right) - \frac{\delta \mathbf{B}}{B} \cdot \nabla (\mu B - e\Phi_{eff}) \frac{v_\parallel f_{0e}}{eT_e} + \mathbf{b}_0^* \cdot \nabla (e\Phi_{eff}) \frac{v_\parallel f_{0e}}{eT_e}, \end{aligned} \quad (2.6)$$

where the velocity space nonlinearity is usually neglected. Here, the electron temperature is given by $T_e = m_e v_{the}^2$ (v_{the} is the electron thermal velocity).

In Eq. (2.6), the lowest order terms (in terms of the square-root of the mass ratio δ_m) are

$$\begin{aligned} v_\parallel \mathbf{b} \cdot \nabla \delta f_e^{(0)} &= \frac{c}{B^2} \mathbf{B} \cdot \nabla f_{0e} \times \left(-v_\parallel \frac{\nabla A_\parallel}{c} \right) + \mathbf{b} \cdot \nabla (e\Phi_{eff}) \frac{v_\parallel f_{0e}}{eT_e} \\ &= -v_\parallel \frac{\partial f_{0e}}{\partial \psi_0} \frac{\partial A_\parallel}{\partial \alpha_0} + v_\parallel \frac{\partial f_{0e}}{\partial \alpha_0} \frac{\partial A_\parallel}{\partial \psi_0} + \mathbf{b} \cdot \nabla (e\Phi_{eff}) \frac{v_\parallel f_{0e}}{eT_e} \\ &= v_\parallel \mathbf{b} \cdot \nabla \frac{\partial f_{0e}}{\partial \psi_0} \delta \psi + v_\parallel \mathbf{b} \cdot \nabla \frac{\partial f_{0e}}{\partial \alpha_0} \delta \alpha + v_\parallel \mathbf{b} \cdot \nabla (e\Phi_{eff}) \frac{f_{0e}}{eT_e}. \end{aligned} \quad (2.7)$$

Employing Eqs. (2.2) and (2.3) [$\partial A_\parallel / \partial \alpha_0 = -\mathbf{b} \cdot \nabla \delta \psi$ and $\partial A_\parallel / \partial \psi_0 = \mathbf{b} \cdot \nabla \delta \alpha$], we obtain the lowest order solution

$$\delta f_e^{(0)} = \frac{e f_{0e}}{T_e} \Phi_{eff} + \frac{\partial f_{0e}}{\partial \psi_0} \delta \psi + \frac{\partial f_{0e}}{\partial \alpha_0} \delta \alpha. \quad (2.8)$$

The first term in Eq. (2.8) represents the Boltzmann response to the parallel electric field. The second and the third term represent the electron thermal equilibration along the perturbed magnetic field. We then separate $\delta f_e = \delta f_e^{(0)} + \delta h_e$. By substituting Eq. (2.8) into Eq. (2.6) and taking the moment of the electron drift kinetic equation (2.6), the continuity equation for the fluid electron is given by

$$\begin{aligned} \frac{\partial \delta n_e}{\partial t} = & -(\mathbf{B}_0 + \delta \mathbf{B}) \cdot \nabla \frac{n_0 \delta u_{\parallel e}}{B_0} - \mathbf{v}_E \cdot \nabla (n_0 + \delta n_e) \\ & - \frac{\mathbf{B}_0 \times \nabla B_0}{m_e \Omega_{ce} B_0^2} \cdot [\nabla \delta p_{\perp e} - n_0 e \nabla \Phi] - \frac{\mathbf{b} \times (\mathbf{b} \cdot \nabla) \mathbf{b}}{m_e \Omega_{ce}} \cdot [\nabla \delta p_{\parallel e} - n_0 e \nabla \Phi], \end{aligned} \quad (2.9)$$

where the pressure terms, $p_{\perp e}$ and $p_{\parallel e}$ are given by

$$\delta p_{\perp e} = \int \mu B \delta f_e d^3 v = n_0 e \Phi_{eff} + \delta \psi \frac{\partial p_{0\perp e}}{\partial \psi_0} + \delta \alpha \frac{\partial p_{0\perp e}}{\partial \alpha_0} + \int \mu B \delta h_e d^3 v, \quad (2.10)$$

$$\delta p_{\parallel e} = \int m_e v_{\parallel}^2 \delta f_e d^3 v = n_0 e \Phi_{eff} + \delta \psi \frac{\partial p_{0\parallel e}}{\partial \psi_0} + \delta \alpha \frac{\partial p_{0\parallel e}}{\partial \alpha_0} + \int m_e v_{\parallel}^2 \delta h_e d^3 v. \quad (2.11)$$

Here, $\int d^3 v$ is the integral over velocity space.

From Eq. (2.8), the lowest order equation for the effective potential is given by

$$\frac{e \Phi_{eff}^{(0)}}{T_e} = \frac{\delta n_e}{n_0} - \frac{\delta \psi}{n_0} \frac{\partial n_0}{\partial \psi_0} - \frac{\delta \alpha}{n_0} \frac{\partial n_0}{\partial \alpha_0}, \quad (2.12)$$

To determine $\delta \psi$ and $\delta \alpha$ in the Clebsch form [24], the following magnetic field equation is solved [instead of solving Eqs. (2.2) and (2.3)],

$$\frac{\partial \delta \psi}{\partial t} = -\mathbf{v}_{\Phi_{ind}} \cdot \nabla \delta \psi + c \frac{\partial \Phi_{ind}}{\partial \alpha_0}, \quad (2.13)$$

$$\frac{\partial \delta \alpha}{\partial t} = -\mathbf{v}_{\Phi_{ind}} \cdot \nabla \delta \alpha + c \frac{\partial \Phi_{ind}}{\partial \psi_0}, \quad (2.14)$$

where $\mathbf{v}_{\Phi_{ind}} = c \mathbf{B}_0 \times \nabla (\Phi_{ind} / B_0^2)$.

One unique feature of the hybrid model [22–25] is to obtain A_{\parallel} by the inverse of the Faraday's law

$$\frac{\partial A_{\parallel}}{\partial t} = c \nabla_{\parallel} (\Phi_{eff} - \Phi). \quad (2.15)$$

The inversion is devised in the hybrid model taking advantage of the lowest order solution Eq. (2.8). As we see in Eq. (2.15), since we enforce the time derivative term to be in a potential form, the $k_{\parallel} = 0$ component of the parallel inductive electric field E_{\parallel} is eliminated. The elimination of the tearing parity mode is solely due to this relation. For Eq. (2.15) to be solvable, Φ_{eff} needs to be a known quantity a priori. Then the notion

of adiabatic electrons in Eqs. (2.8) and (2.19) plays a role. The elimination of the tearing parity mode is a direct consequence of the asymptotic expansion by δ_m and remains the same even with the inclusion of non-adiabatic kinetic electrons as long as the specific mode " $E_{\parallel}(k_{\parallel}=0)$ " is absent in Eq. (2.18). We demonstrate this feature in Section 3 [As a comparison, the split weight scheme [29–31] contains full drift kinetic physics of Eq. (2.6)].

Discussed above are the dynamical equations which are evolved in time. To complete the hybrid model, we solve the following field equations. The gyrokinetic Poisson equation is given by

$$-\frac{\tau}{\lambda_d^2}(\Phi - \tilde{\Phi}) = -4\pi e(\delta\bar{n}_i - \delta n_e), \quad (2.16)$$

where $\tilde{\Phi}$ is the double gyro averaged electrostatic potential [19]. Here $\tau = T_e/T_i$ (T_i is the ion temperature) and λ_d is the Debye length. In Eq. (2.16), $\delta\bar{n}_i = (1/n_0) \int \delta f_i d^3v$. The Ampere's law is inverted to obtain the parallel electron current

$$n_0 e \delta u_{e\parallel} = \frac{c}{4\pi} \nabla_{\perp}^2 A_{\parallel} + n_0 e \delta \bar{u}_{i\parallel} \quad (2.17)$$

which will then enter Eq. (2.9). Here, $\delta \bar{u}_{i\parallel} = (1/n_0) \int v_{\parallel} \delta f_i d^3v$.

Substituting $\delta f_e = \delta f_e^{(0)} + \delta h_e$ into Eq. (2.6) and keeping higher order terms we obtain the electron kinetic equation for the non-adiabatic response δh_e

$$\begin{aligned} \frac{d\delta h_e}{dt} = & c \frac{\partial f_{0e}}{\partial \psi_0} \frac{\partial \Phi}{\partial \alpha_0} - c \frac{\partial f_{0e}}{\partial \alpha_0} \frac{\partial \Phi}{\partial \psi_0} - \frac{e f_{0e}}{T_e} \frac{\partial \Phi_{eff}^{(0)}}{\partial t} - \frac{\partial f_{0e}}{\partial \psi_0} \frac{\partial \delta \psi}{\partial t} - \frac{\partial f_{0e}}{\partial \alpha_0} \frac{\partial \delta \alpha}{\partial t} \\ & - (\mathbf{v}_E + \mathbf{v}_g + \mathbf{v}_c) \cdot \nabla \left(\frac{\partial f_{0e}}{\partial \psi_0} \delta \psi + \frac{\partial f_{0e}}{\partial \alpha_0} \delta \alpha \right) \\ & - \mathbf{v}_g \cdot \nabla \left(\frac{e f_{0e}}{T_e} \Phi_{eff}^{(0)} \right) + \mathbf{v}_E \cdot \nabla \left(\frac{e f_{0e}}{T_e} \Phi_{ind} \right). \end{aligned} \quad (2.18)$$

We then employ the relation

$$\frac{e \Phi_{eff}^{(1)}}{T_e} = - \frac{\delta n_e^{(1)}}{n_0} \quad (2.19)$$

to obtain $\Phi_{eff} = \Phi_{eff}^{(0)} + \Phi_{eff}^{(1)}$, which then enters Eq. (2.15). Here,

$$\delta n_e^{(1)} = \frac{1}{n_0} \int \delta h_e d^3v.$$

The higher order kinetic effect enters the system through $\Phi_{eff}^{(1)}$, Eqs. (2.10) and (2.11) (and not through the gyrokinetic Poisson equation).

The δf gyrokinetic equation is solved for the kinetic ions (here, we separate the ion distribution function $f_i = f_{0i} + \delta f_i$)

$$\begin{aligned} \frac{d\delta f_i}{dt} = & \frac{c}{B^2} \mathbf{B} \cdot \nabla f_{0e} \times \left(\nabla \Phi - v_{\parallel} \nabla \frac{A_{\parallel}}{c} \right) \\ & - \frac{\delta \mathbf{B}}{B} \cdot \nabla (\mu B - e\Phi_{eff}) \frac{v_{\parallel} f_{0i}}{eT_i} + \mathbf{b}_0^* \cdot \nabla (e\Phi_{eff}) \frac{v_{\parallel} f_{0i}}{eT_i}, \end{aligned} \quad (2.20)$$

where the magnetic moment is defined by $\mu = m_i v_{\perp}^2 / 2B$. All the perturbed quantities in Eq. (2.20) are gyro-phase averaged values.

3 Electromagnetic simulations with kinetic electrons

In this section we present electromagnetic gyrokinetic simulation with kinetic electrons using the hybrid model employing the GTC code [2]. As a reference, kinetic electrons have been included in linear [7] and nonlinear [26] toroidal simulations with magnetic shear using an electrostatic version of the hybrid model, which employs the same expansion by the square-root of the electron-ion mass ratio. These simulations [7,26] show that there is no numerical difficulty of electron response near mode rational surfaces; the tearing parity mode is not destabilized which is a natural consequence of the hybrid model formulation which theoretically removed the tearing parity modes.

The gyrokinetic toroidal code GTC is based on the gyrokinetic particle in cell (PIC) approach which allows efficient sampling of the velocity space [18,19]. The GTC code takes an initial value approach which dynamically evolves gyrokinetic equations and the field equations (either electrostatic or electromagnetic). The field equations are solved in the real space which allows implementations of realistic boundary conditions. We also employ the global field aligned mesh [32] which rotates in the toroidal direction together with the resonant mode at each rational surface and thus the mesh structure is not axisymmetric. When we employ the global field aligned mesh, we no longer have an advantage of having a logically rectangular mesh since each radial surface rotates at a different pitch due to the finite magnetic shear. The consequent logically non-rectangular mesh in GTC also keeps the numbers of particle per cell to be constant which is favorable for the statistical estimation of the charges and the currents. The original GTC code [2] with adiabatic electrons is extended to include kinetic electrons by the hybrid approach [7,26] and the effort to include split-weight approach is reported [33] in the electrostatic limit [29]. Furthermore, the extension to shaped plasmas (in the adiabatic electron limit) is reported in [34,35]. The electromagnetic capability in a circular cross section is demonstrated in [25].

The parameters used below are toroidal magnetic field $1.91T$, equilibrium ion and electron temperature $T_i = T_e = 2500eV$. The plasma size is given by the major radius $R = 46.6 \text{ cm}$ and the minor radius $a = 16.7 \text{ cm}$. The density gradient and the ion temperature gradient are given by $\kappa_n = -R(d\log(n)/dr) = 2.22$, $\kappa_{Ti} = -R(d\log(T_i)/dr) = 6.92$, and

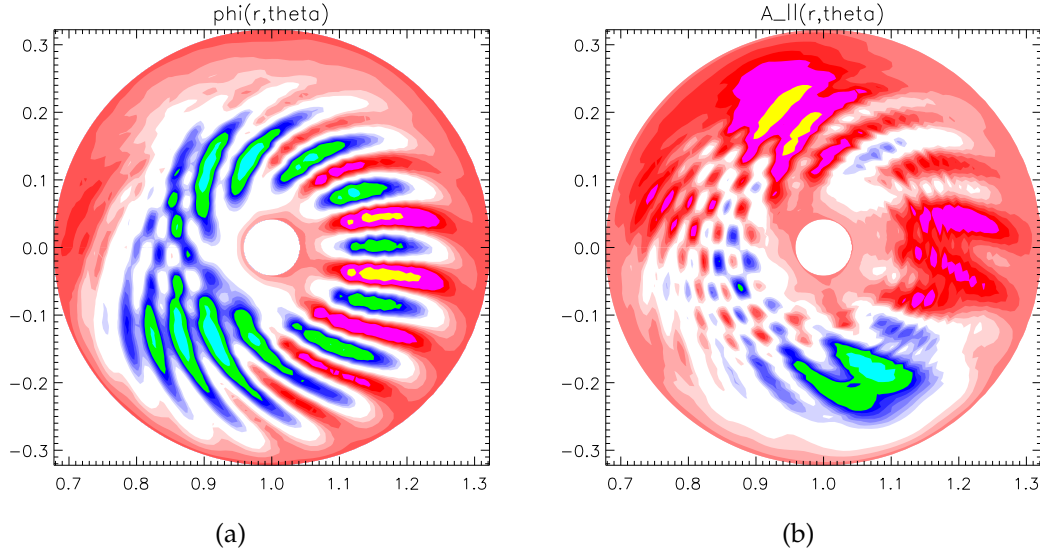


Figure 1: Simulation results with kinetic electrons. (a) Φ and (b) A_{\parallel} contours. Here, $\beta_e = 0.5\%$.

$\kappa_{te} = -R(d\log(T_e)/dr) = 6.92$. Here, r is the radial coordinate which relates to the flux label $\psi_0 = \int B_0(r/q)dr$. The magnetic shear at the midplane is 0.776 with a safety factor of 1.4 as in the Cyclone base case [1]. Shown in Fig. 1 are the simulation results in the presence of kinetic electrons with the electron plasma beta value of $\beta_e = 0.5\%$. In Fig. 1, the linear eigenfunction of the finite- β modified ITG is shown. Note that the radial profile of Φ has even parity across the mode rational surfaces, while A_{\parallel} has odd parity as in Fig. 8 of [25]. The parity of Φ is that of the ion temperature gradient mode (ITG) and the A_{\parallel} parity simply follows the opposite of Φ . The radial eigenmode structure of Φ is known to take the form of Weber function [9, 36] [superpositions of Gaussian function (the *even* parity) localized at each mode rational surface] and the streamer, or finger-like, feature is seen as in Fig. 1(a). On the contrary, we observe discontinuous (wavy) features in Fig. 1(b), since the radial eigenmode structure changes its sign across each mode rational surface (the *odd* parity). In Fig. 1, tearing parity mode is not excited which is the nature of the hybrid model formulation as we discussed in the previous section. The tearing parity mode is always present (at the white noise level) but does not grow.

The linear growth rate and the real frequency of the finite beta modified ITG mode is shown in Fig. 2 (as a function of β_e). The Fourier modes included in this simulation are all the poloidal m modes and a single toroidal mode $n = 9$ (the rest of the n modes are filtered out).

We observe the onset of kinetic ballooning mode at $\beta_e \geq 0.7\%$. The absolute values of the real frequency (which are the negative values) increases at $\beta_e \geq 0.7\%$ and then decrease with a further increment in β_e . Finite beta stabilization at $\beta_e \leq 0.7\%$ is not as prominent as reported by [37, 38].

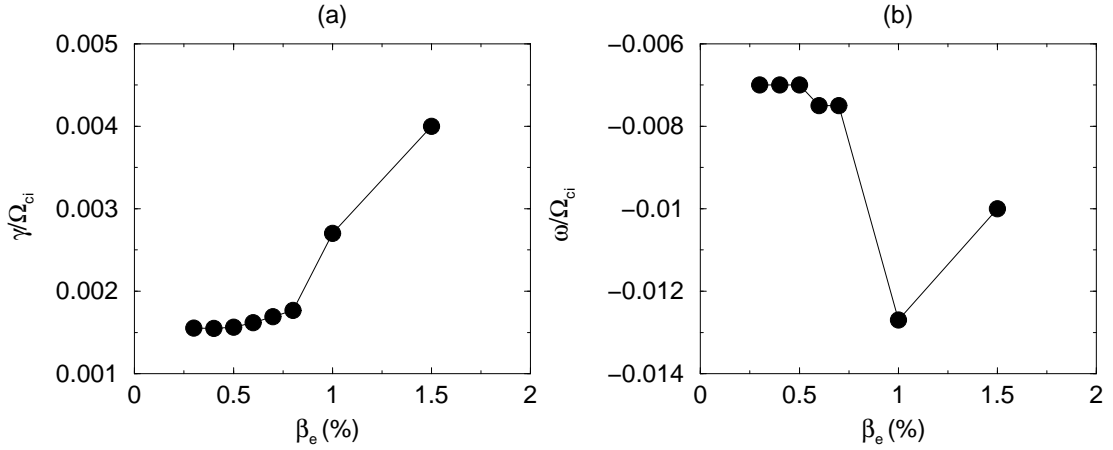


Figure 2: The β_e dependence of finite beta modified ITG (a) linear growth rates and (b) real frequency for $n=9$. Here, $T_i=T_e=250eV$, $R=46.6$ cm, $\kappa_n=2.22$, $\kappa_{ti}=6.92$, and $\kappa_{te}=6.92$. The values are normalized by ion cyclotron frequency Ω_{ci} .

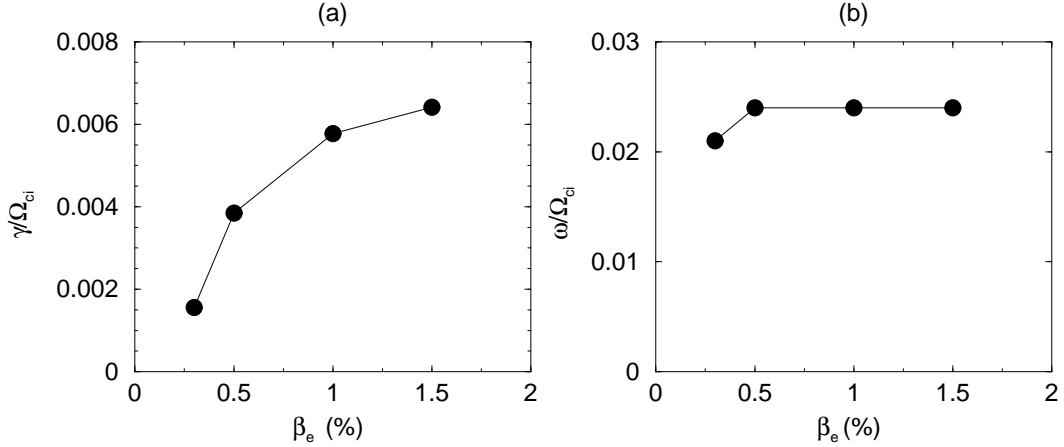


Figure 3: The β_e dependence of (a) linear growth rates and (b) real frequencies for $n=7$ modes. Here, $T_i=T_e=250eV$, $R=23.3$ cm, $\kappa_n=2.0$, $\kappa_{ti}=2.0$, and $\kappa_{te}=7.0$. The values are normalized by ion cyclotron frequency Ω_{ci} .

The linear growth rate and the frequency with a smaller ion temperature gradient parameter is shown in Fig. 3 (versus the β_e value). The parameters used below in Figs. 3 and 4 employs relatively small number of mesh points. Here, we take 24 radial mesh points, 88 poloidal mesh points on the midplane, and 16 toroidal mesh points in the global field aligned non-rectangular mesh (as a comparison, in Figs. 1 and 2, 48, 176, and 32 are taken for the radial, the midplane poloidal, and toroidal mesh points, respectively). The plasma size is given by the major radius $R=23.3$ cm and the minor radius $a=8.3$ cm, with a toroidal magnetic field 1.91T and equilibrium ion and electron temperature of $T_i=T_e=250eV$. The density gradient, the ion temperature gradient, and the electron temperature gradient are given by $\kappa_n=2.0$, $\kappa_{ti}=2.0$, and $\kappa_{te}=7.0$. The filtered toroidal

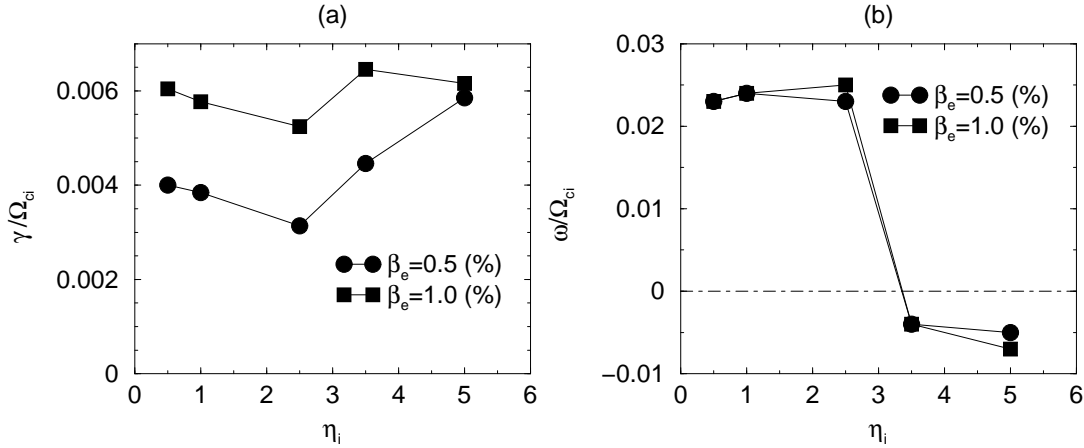


Figure 4: The η_i dependence of finite beta modified modes (corresponds to ITG at $\eta_i \geq 3.0$). Plotted are (a) linear growth rates and (b) real frequencies for the $n=7$ modes. The values are normalized by ion cyclotron frequency Ω_{ci} .

mode number is $n=7$. We see a monotonic increase in the linear growth rate and the real frequency is almost constant over the range of $0.3\% \geq \beta_e \geq 1.5\%$. Further detailed study is required to identify if the mode is the trapped electron mode.

Shown in Fig. 4 are the linear growth rate and real frequency versus $\eta_i = \kappa_{ti} / \kappa_n$ for beta values of $\beta_e = 0.5\%$ (filled circles) and $\beta_e = 1.0\%$ (filled squares). The density gradient $\kappa_n = 2.0$ and the electron temperature gradient $\kappa_{te} = 7.0$ are fixed. The methodology is taken from Fig. 4 of [7] in the electrostatic case. A transition is seen near $\eta = 3.0$, possibly from the trapped electron mode to the ITG mode [7]. At $\eta_i = 5.0$, the magnitude of the linear growth rate and the real frequency becomes comparable [uncertainty in the measured values as seen in the square plot at $\eta_i = 5.0$ in Fig. 4(a)]. Detailed investigation of the trapped electrons modes (TEM) in the electromagnetic regime will be our next step task.

Our initial electromagnetic gyrokinetic particle simulation results with kinetic electrons in the presence of magnetic shear is successfully demonstrated without the destabilization of the tearing parity modes. These simulation results show that there is no numerical difficulty of electron response near mode rational surfaces.

4 Summary and discussions

In this paper, electromagnetic gyrokinetic particle simulations using the hybrid model with kinetic electrons are presented. The simulation is performed in a global full torus geometry in the presence of magnetic shear. We reported our initial studies on the parameter dependence of the electromagnetic drift wave instabilities in the presence of kinetic electrons. We have discussed the onset of kinetic ballooning mode in the presence of large ion temperature gradient drive. We have also studied cases with large electron temperature gradient drive that possibly correspond to the trapped electron mode [7]. By varying

the η_i value, the real frequency changes its sign as manifested in the electrostatic studies [7]. More detailed investigation (the detailed parameter scan) of the trapped electrons modes (TEM) in the electromagnetic regime will be our particular interest. We plan to compare the simulation results with the eigenvalue calculations.

As we discussed above the current hybrid model removes collisionless tearing modes and thus magnetic stochasticity induced parallel electron heat transport cannot be described. While the collisionless reconnection is eliminated, the hybrid model is capable of simulating resistive reconnection. Whether we can include tearing parity modes (question is how to include the $k_{\parallel}=0$ mode of the parallel inductive electric field E_{\parallel}) is opened for further discussions.

While the electrostatic fluid-kinetic hybrid model requires time centering scheme in the electron drift kinetic equation, the electromagnetic hybrid model presented in this paper is free from time centering due to the lowest order electron continuity equation (as a comparison, electrostatic split weight scheme avoids time centering scheme but then requires an additional Poisson type equation for the time derivative of the electrostatic potential).

Acknowledgments

This work is supported by Department of Energy (DOE) Cooperative Agreement No. DE-FC02-04ER54796, Grant No. DE-FC02-06ER54860, and in part by SciDAC GPS, GSEP, and CPES centers. YN would like to thank Dr. T. S. Hahm, Dr. E. A. Startsev, and Dr. W. X. Wang for useful discussions.

References

- [1] A. Dimits et al., *Phys. Plasmas* **7**, 969 (2000).
- [2] Z. Lin, T. S. Hahm, W. W. Lee, W. M. Tang, and R. B. White, *Science* **281**, 1835 (1998).
- [3] B. Coppi, *Phys. Fluids* **10**, 582 (1967).
- [4] A. Hasegawa and M. Wakatani, *Phys. Rev. Lett.* **59**, 1581 (1987).
- [5] W. M. Tang, *Nucl. Fusion* **18**, 1089 (1978).
- [6] G. Rewoldt, W. M. Tang, and R. J. Hastie, *Phys. Fluids* **30**, 807 (1987).
- [7] G. Rewoldt, Z. Lin, and Y. Idomura, *Comput. Phys. Comm.* **177**, 775 (2007).
- [8] A. B. Rechester and M. N. Rosenbluth, *Phys. Rev. Lett.* **40**, 38 (1978).
- [9] Y. Nishimura and M. Azumi, *Phys. Plasmas* **4**, 2365 (1997).
- [10] W. Horton, *Phys. Fluids* **31**, 2971 (1988).
- [11] F. Jenko and W. Dorland, *Phys. Plasmas* **7**, 1904 (2000).
- [12] Z. Lin, L. Chen, and F. Zonca, *Phys. Plasmas* **12**, 056125 (2005).
- [13] C. Z. Cheng, L. Chen, and M. S. Chance, *Ann. Phys. (N.Y.)* **161**, 21 (1985).
- [14] C. Z. Cheng and M. S. Chance, *Phys. Fluids* **29**, 3695 (1986).
- [15] F. Zonca, L. Chen, R. A. Santoro, and J. Q. Dong, *Plasma Phys. Controlled Fusion* **40**, 2009 (1998).
- [16] G. Zhao and L. Chen, *Phys. Plasmas* **9**, 861 (2002).

- [17] C. Z. Cheng, Phys. Fluids **25**, 1020 (1982).
- [18] W. W. Lee, Phys. Fluids **26**, 556 (1983).
- [19] W. W. Lee, J. Comput. Phys. **72**, 243 (1987).
- [20] J. C. Reynders, Ph.D. dissertation, Princeton University (1992).
- [21] J. C. Cummings, Ph.D. dissertation, Princeton University (1995).
- [22] Z. Lin and L. Chen, Phys. Plasmas **8**, 1447 (2001).
- [23] W. X. Wang, L. Chen, and Z. Lin, Bull. Am. Phys. **46**, 114 (2001).
- [24] F. L. Hinton, M. N. Rosenbluth, and R. E. Waltz, Phys. Plasmas **10**, 168 (2003).
- [25] Y. Nishimura, Z. Lin, and W.X.Wang, Phys. Plasmas **14**, 042503 (2007).
- [26] Z. Lin, *et al.*, Plasma Phys. Controlled Fusion **49**, B 163 (2007).
- [27] Y. Lin, X. Wang, Z. Lin and L. Chen, Plasma Phys. Controlled Fusion **47**, 657 (2005).
- [28] A. J. Brizard and T. S. Hahm, Rev. Mod. Phys. **79**, 421 (2007).
- [29] I. Manuilskiy and W. W. Lee, Phys. Plasmas **7**, 1381 (2000).
- [30] W. W. Lee, J. L. V. Lewandowski, T. S. Hahm, and Z. Lin, Phys. Plasmas **8**, 4435 (2001).
- [31] Y. Chen and S. Parker, Phys. Plasmas **8**, 2095 (2001).
- [32] B. Scott, Phys. Plasmas **5**, 2334 (1998).
- [33] J. L. V. Lewandowski *et al.*, Phys. Plasmas **13**, 072306 (2006).
- [34] J. L. V. Lewandowski, A. Boozer, J. Williams, Z. Lin, M. Zarnstorff, Bull. Am. Phys. **45**, (2000).
- [35] W. X. Wang *et al.*, Phys. Plasmas **13**, 092505 (2006).
- [36] M. Abramowitz and I. A. Stegun, *Handbook of Mathematical Functions*, (Dover, New York, 1970), p.498.
- [37] Y. Chen and S. Parker, J. Comput. Phys. **189**, 463 (2003)
- [38] J. Candy and R. E. Waltz, J. Comput. Phys. **186**, 545 (2003).